Eur Biophys J (2008) 38:25–35
DOI 10.1007/s00249-008-0350-8

ORIGINAL PAPER

Comparative structural dynamics of Tyrosyl-tRNA synthetase complexed with different substrates explored by molecular dynamics

Tong Li · Matheus Froeyen · Piet Herdewijn

Received: 7 April 2008 / Revised: 27 May 2008 / Accepted: 4 June 2008 / Published online: 17 June 2008

Abstract Several molecular dynamics simulations of *S. aureus* Tyrosyl-tRNA synthetase (TyrRS) in its free form and complexed with Tyr, ATP, tyrosyl adenylate and inhibitor respectively have been carried out to investigate the ligand-linked conformational stability changes associated with its catalytic cycle. The results show that unliganded *S. aureus* TyrRS samples a more relaxed conformational space than substrate-bound TyrRS. There are three high flexibility regions encompassing residues 114–118, 128–133, and 226–238 respectively. The region which includes the KMSKS motif (KFGKS in *S. aureus* TyrRS) shows the highest difference in fluctuations. Hydrogen bond network formed by Tyr, ATP, tyrosyl adenylate and inhibitor with *S. aureus* TyrRS is discussed. Our simulations suggest the induced-fit conformational changes of the KMSKS loop as follows: the KMSKS loop of substrate-free *S. aureus* TyrRS adopts an open conformation. The tyrosine binds in the pocket with the KMSKS loop balancing between semi-open and open forms. The ATP binding induces the KMSKS loop to the open form. After the Tyr-AMP is formed, the first two residues of KMSKS loop twists in an anticlockwise direction and drives the loop in a conformation similar to the closed one, while those of the last three GKS residues adopt a conformation between semi-open and open conformation. This conformational change may probably be involved in the initial tRNA binding.

Keywords Tyrosyl-tRNA synthetase · Aminoacyl-tRNA synthetases · KMSKS · Molecular dynamics · Hydrogen bond

Introduction

Aminoacyl-tRNA synthetases (aaRSs) play an essential role in protein synthesis by catalyzing the condensation of an amino acid with its cognate tRNA. There are two steps in the process of the catalysis. In the first step, an activated aminoacyl-adenylate intermediate is formed, followed by the charging of the 3′-end of the cognate tRNA in the second step. Based on their structural features, aaRSs are ranked in two classes. Class I synthetases contain a typical Rossman fold in the active site, with the HIGH and KMSKS motifs that stabilize the transition state of the reaction for amino acid activation using ATP-binding energy (Winter et al. 1983; Hountondji et al. 1986; Eriani et al. 1990). Class II enzymes harbor an antiparallel β-sheet domain that provides a rigid template for amino acid and ATP binding, with three characteristic motifs required for dimerization and substrate binding (Ibba and Soll 2000). aaRSs have been and are still essential and promising targets for new anti-infective agents (Ochsner et al. 2007). Numerous high-throughput screening programs aimed at identifying aaRS inhibitors have been performed over the last 20 years (Ochsner et al. 2007). The deep understanding of the catalytic mechanisms of aaRS will facilitate the development of new antibiotic agents.

Tyrosyl-tRNA synthetase (TyrRS) belongs to the class I synthetases, characterized by a Rossmann fold in the

Electronic supplementary material The online version of this article (doi:10.1007/s00249-008-0350-8) contains supplementary material, which is available to authorized users.

T. Li (✉) · M. Froeyen · P. Herdewijn
Laboratory for Medicinal Chemistry,
Rega Institute for Medical Research,
Katholieke Universiteit Leuven,
Minderbroedersstraat 10, 3000 Leuven, Belgium
e-mail: tong.li@rega.kuleuven.be

catalytic domain and the HIGH and KMSKS motifs for ATP binding. It was the first synthetase to have its crystal structure solved including its substrate complexes with tyrosine and tyrosyl-adenylate (Bhat et al. 1982; Brick and Blow 1987; Brick et al. 1989). The two-step catalysis reaction has been formulated in the following equations.

$$\text{TyrRS} + \text{Tyr} + \text{ATP} \rightarrow \text{TyrRS} \cdot \text{Tyr-AMP} + \text{PP}_\text{i}. \quad (1)$$

$$\text{TyrRS} \cdot \text{Tyr-AMP} + \text{tRNA}^{\text{Tyr}} \rightarrow \text{TyrRS} + \text{AMP} + \text{Tyr - tRNA}^{\text{Tyr}}. \quad (2)$$

The Rossmann fold domain binds the amino acid and ATP substrates, and catalyzes the first step of the aminoacylation reaction. Tyrosine substrate is activated by ATP to form an enzyme-bound tyrosyl-adenylate intermediate and then the activated tyrosine is transferred from the tyrosyl-adenylate intermediate to tRNA^{tyr}. A single tRNA^{tyr} molecule is bound per dimer, with the Rossmann fold domain in one subunit recognizing the 3′ end of tRNA^{tyr} and the carboxyl-terminal domain of the other subunit binding the anticodon loop (Qiu et al. 2001; Kobayashi et al. 2005; Carter et al. 1986; Xin et al. 2000). Previous experimental studies (Kobayashi et al. 2005; Yaremchuk et al. 2002; Fersht et al. 1988) have also revealed that the extensive induced-fit conformational changes of the KMSKS loop and the local conformational changes within the substrate binding site form the basis for driving the amino acid activation step: the KMSKS loop adopts the "open" form, transiently shifts to the "semi-open" conformation according to the adenosyl moiety binding, and finally assumes the rigid ATP-bound, "closed" form. After the amino acid activation, the KMSKS loop adopts the "semi-open" form again to accept the CCA end of tRNA for the aminoacyl transfer reaction (Kobayashi et al. 2005).

Many aaRSs such as methionyl-tRNA synthetase (Budiman et al. 2007), aspartyl-tRNA synthetase (Thompson et al. 2006; Thompson and Simonson 2006), lysyl-tRNA synthetase (Hughes et al. 2006) and tryptophanyl-tRNA synthetase (Kapustina and Carter 2006) have been investigated using molecular dynamics (MD) simulation, which has provided us considerably useful dynamical information of aaRSs. MD potentially provide access to two different types of otherwise unavailable information: (1) relative protein stabilities of different conformational states, with and without ligands; and (2) pathways for conformational changes and how they are affected by ligands (Kapustina and Carter 2006). Furthermore, simulations provide potentially useful data for configurations that have not been observed because they are unstable in solution, and for which structures cannot be determined (Kapustina and Carter 2006).

Despite numerous TyrRS structures with or without different substrates were solved, the contribution of protein flexibility to function is poorly understood. Moreover, most of the dynamical information of KMSKS loop comes from the comparison of crystal structures among the same or different species and seldom from the comparison of dynamical structures in the same species. Thus, we have performed MD simulations of *S. aureus* TyrRS, with different substrates modeled in its active site to explore the ligand-linked conformational stability changes associated with its catalytic cycle. The comparison of the dynamics between the different complex systems is of particular interest, as the different change of the conformations of parts of the protein alters in according with the different binding of the substrates. The active sites of TyrRS are well conserved and the orientation of the tyrosine and ATP moieties is very similar in different species (Bonnefond et al. 2005; Kobayashi et al. 2003), therefore, it is reasonable to fit the complex structures of different species having different substrates in the active site, onto the structure of *S. aureus* TyrRS. Our computational studies of TyrRS suggest a clear catalysis mechanism of the activation of the tyrosine and deepen the physical interpretation of experimentally observed conformational changes of the KMSKS loop.

Materials and methods

Initial structures for simulations

The protein structures of the five simulated systems are obtained from the X-ray structure of *S. aureus* TyrRS (Fig. 1) in complex with SB284485 inhibitor determined at 2.20 Å resolution (Protein Data Bank (Berman et al. 2000) code 1JIL). *S. aureus* TyrRS monomer contains three domains: the N-terminal α/β domain (1–220), the α-helical domain (248–323) and the C-terminal domain (324–421). The N-terminal α/β domain and the α-helical domain are connected via a linker peptide (LP) (221–247). Due to the disorder of the C-terminal domain (324–421) in the crystal, the X-ray structure does not include the residues 325–421 (Brick et al. 1989). The C-terminal domain is distant from the binding site of the substrates Tyr, ATP and tyrosyl adenylate and the main aspect that we try to explore is the conformational dynamics of residues from the binding site and its neighbor during substrate binding, therefore it is reasonable to use the truncated version to replace the full version of this enzyme. The residues KFGKS (231–235) form the KMSKS motif in *S. aureus* TyrRS.

The unliganded TyrRS system was obtained by deleting inhibitor (SB284485) from the crystal structure 1JIL. The Tyr-bound, ATP-bound, and tyrosyl-adenylate-bound TyrRS systems were defined through building them into the binding site of TyrRS separately (Table 1). The conformations of these three substrates were taken from other crystal structures because the catalytic domains of all

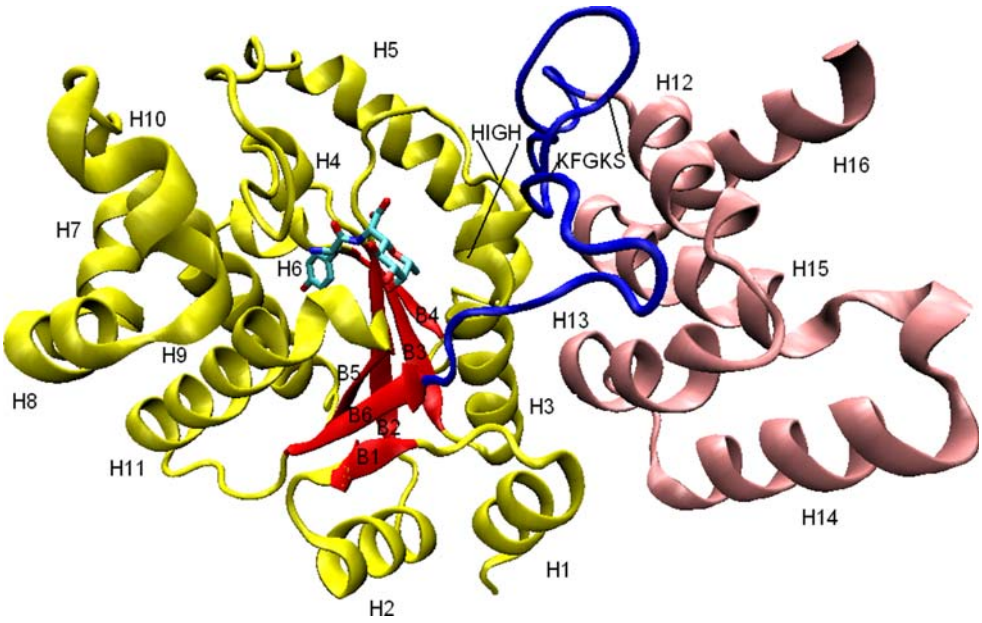

Fig. 1 Newcartoon representation of the monomeric form of *S. aureus* TyrRS. C-terminal domain is omitted. The N-terminal domain is in *yellow* (helices) and *red* (strands), the linker peptide in *blue* and α-helical domain in *pink*. The inhibitor SB284485 is shown in licorice model colored according to the element (carbon in *cyan*, nitrogen in *blue* and oxygen in *red*). Helices and strands are named in sequence order. *H* stands for α-helix and *B* stands for *β*-strands. HIGH (47–50) and KMSKS (231–235) motif are also shown

bacterial TyrRSs are conserved and the substrates have similar binding modes in the binding pocket of different species of TyrRS (Bonnefond et al. 2005; Kobayashi et al. 2003; Retailleau et al. 2001).

Molecular dynamics simulations

All simulations were conducted by using the AMBER 9 program (Pearlman et al. 1995; Case et al. 2006). The ligands except Tyr were prepared by using the antechamber suite (Wang et al. 2004) in the AMBER package. Atomic charges were derived with the AM1-BCC charge method (Jakalian et al. 2000). Two parameter sets were used, the biomolecular force field ff03 (Duan et al. 2003) for the protein and general AMBER force field (Wang et al. 2004) for the ligands. For each simulation, the same simulation step was taken as described below. The complex was soaked in a truncated octahedron box of TIP3P (Jorgensen et al. 1982, 1983) water molecules with a margin of 10 Å along each dimension using the LEAP module. Na^+ ions were added to neutralize the system. These yielded about 44,800 atoms for each simulation. These systems were minimized by 200 steps of steepest descent followed by 800 steps of conjugate gradient to remove the bad contacts in the crystal structure. During the minimization, a 12 Å non-bonded cutoff was applied. These systems were then heated from 0 to 300 K in 40 ps. A subsequent 12 ns production run was performed at a constant temperature of 300 K and a constant pressure of 1 atm after 200 ps of equilibration. The time interval was set to 2 fs. The Particle Mesh Ewald method (Darden et al. 1993) was applied to calculate long-range electrostatics interactions. The SHAKE method (Ryckaert et al. 1977) was applied to constrain all of the covalent bonds involving hydrogen

Table 1 Initial systems for molecular dynamics simulations

Simulation systems	Ligands	Construction
Unliganded TyrRS		Constructed by ligand removal
TyrRS + Tyr	4TS1	Constructed by superposition of 1JIL and 4TS1, keeping the protein of 1JIL and Tyr ligand of 4TS1
TyrRS + ATP	1H3E	Constructed by superposition of 1JIL and 1H3E, keeping the protein of 1JIL and ATP ligand of 1H3E
TyrRS + tyrosyl-adenylate	3TS1 + 1I6 K	Constructed by adding the Trp carboxylate oxygen of tryptophanyl-adenylate ligand of 1I6 K to the same position of tyrosinyl-adenylate ligand of 3TS1, superposing 1JIL with 3TS1 and keeping the protein of 1JIL and tyrosyl-adenylate ligand of 3TS1
TyrRS + inhibitor (SB284485)	1JIL	

The proteins in the five simulated systems are all extracted from the 1JIL

atoms. Periodic boundary conditions were applied to all dimensions. No constraint was applied to either the protein or the ligand during MD simulation. Coordinates were saved at 0.4 ps intervals along the 12 ns production runs.

Analysis

An extra 2 ns MD was performed for the unliganded TyrRS system after checking the root-mean-square deviation (RMSD) plot of C_α atoms relative to the starting minimized structure to obtain stability. An average structure of the last 5 ns trajectories for each simulation was calculated using the *PTRAJ* module of AMBER and minimized using the same protocol as that used before the molecular dynamics. Criteria for identifying hydrogen bonds were as follows: (1) the distance between proton donor (X) and acceptor (Y) atoms was less than or equal to 3.5 Å, (2) the angle X–H…Y was greater than or equal to 120°. These hydrogen bonds that persisted throughout at least 40% of the analyzed period were given special attention. In order to validate the robustness of our simulated systems, extra five simulations were conducted with different starting points and initial velocities for every system. The last snapshot from the end of 6 ns production simulation of each system was used as a new starting point to start independent simulations. All the systems were reheated from 0 to 300 K in 40 ps and continued for 5 ns (6 ns for unliganded TyrRS) production run. In general, the results from the validation simulations were compatible with those from our original simulations and each trajectory displayed essentially the same behavior, which showed that our simulation protocol was reliable. The RMSD plot of the validation simulations and the superposition of average structures from validation simulations with those from our original simulations can be found in the Supplementary material respectively (Fig. S1 and S2).

To determine the influence of macromolecular association on the magnitude of motions, the root mean square amplitude of motion of atoms about their mean positions was determined from the last 5 ns MD trajectory in the *PTRAJ* module. Experimental RMSFs about the mean position of atom i can be estimated from the crystallographic temperature factor B_i (Gohlke et al. 2004; McCammon and Harvey 1987)

$$\left\langle u_i^2 \right\rangle^{1/2} = \left(3B_i/8\pi^2\right)^{1/2}. \quad (3)$$

The calculated radius of gyration (R_g) monitors the changes in the "compactness" of the protein during the simulations. A decrease in R_g in simulations indicates the physical rearrangement of an elongated protein to a more globular structure, and has also been interpreted to indicate an increase in the protein's packing density (Dadarlat and Post 2001).

Finally, for each of the five simulated systems from the last 5 ns MD trajectories at a 1 ns interval, were extracted and compared to the structures of *E. coli* TyrRS·tyrosine, *E. coli* TyrRS·Tyr-AMS and *T. thermophilus* TyrRS·ATP·tyrosinol·tRNA^{Tyr} after superposition. The conformational changes of the KMSKS loop were analyzed. All the superposition was performed in Chimera (Pettersen et al. 2004).

Results and discussion

Structural stability during the simulations

The RMSDs of the C_α atoms of all the simulations from the starting minimized structure were monitored to detect the conformational stability and structural changes (Fig. 2). The unliganded TyrRS simulation deviates further than any other system from its starting conformation. The RMSD curve of unliganded system can be clearly divided into three parts: it increases quickly to about 1.8 Å before ~3 ns. Then it tends to be partially stable from 3 to 9 ns and the average RMSD of this period is about 2.4 Å. In the end from 9 to 14 ns, it reaches full equilibration and the average RMSD for this period is about 2.6 Å. For the other four simulations, the plot shows that the equilibrations are reached much earlier than in the unliganded system and the average RMSDs of the last 5 ns simulation (7–12 ns) for the four systems are around 1.7–2.1 Å. The unliganded TyrRS samples more conformational space than those of substrate-bound TyrRSs compared to the starting structure. According to the statistical analysis of the RMSD data, the last 5 ns simulations of each system which are more stable are selected to do further analysis.

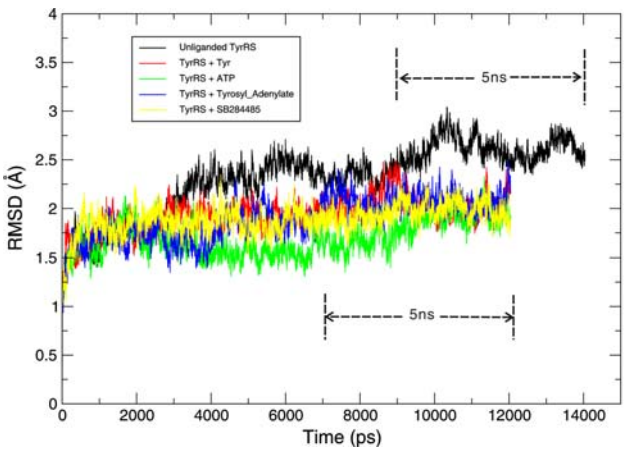

Fig. 2 RMSDs of C_α atoms from the initial configuration for the five simulated trajectories

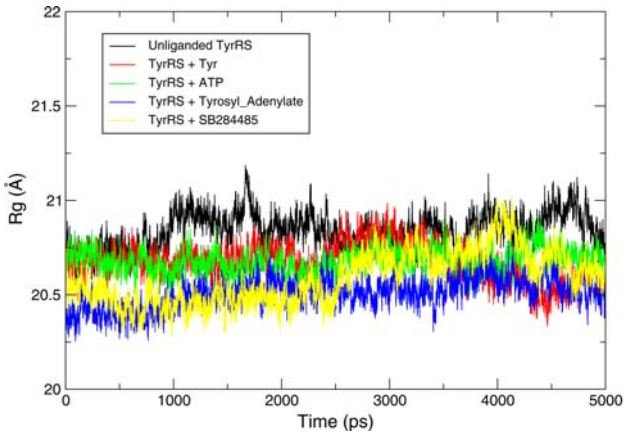

Fig. 3 Time evolution of the R_g for the five simulated TyrRS systems during the last 5 ns simulation period

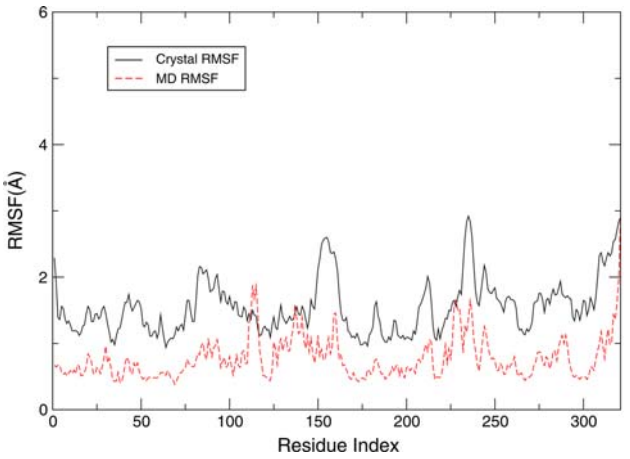

Fig. 4 Comparison of RMSF of C_α atoms per residue derived from the SB284485-bound TyrRS simulation and crystallographic data of 1JIL

The radius of gyration (R_g) of the five systems along the last 5 ns simulations is shown in Fig. 3. The average R_g values of the five systems vary slightly from about 20.4–20.8 Å, indicating that there is no distinct alternation in structure compactness along the last 5 ns simulation period. The unliganded TyrRS has the largest R_g value of the five systems, which shows it samples the most relaxed space compared to other substrate-bound enzymes. From the substrate-bound TyrRS systems, the Tyr- and ATP-bound TyrRS systems have slightly higher R_g values. Overall, the binding of different substrates reduce the R_g values and slightly increase the compactness of the enzyme slightly compared to the unliganded TyrRS. Furthermore, the R_g plots indicate that the volumes occupied by the conformations sampled in the five systems are similar and the simulations are stable in the last 5 ns period.

Residue flexibility

The intrinsic flexibility of a crystal structure is manifested by the B-factors of the atomic coordinates, which therefore can provide validation for MD trajectories based on experimentally determined structures (Kapustina and Carter 2006). The RMSFs of the SB284485-bound TyrRS system obtained from the simulation have been compared to the corresponding values calculated from the experimental B factors in its crystal structure, which is shown in Fig. 4. The experimental B factors are transformed into the RMSFs using Eq. (3). Our analysis did not include the residue 323 and 324 because of the high flexibility of these two residues possibly originating from the missing C-terminal domain.

As Eq. (3) ignores effects due to static disorder also present in the crystal, the baseline of the experimental B-factors is higher than those determined from the simulations (Kapustina and Carter 2006). The overall pattern of fluctuations taken from the MD is close to that observed from the crystallographic B-factors. Nevertheless, there is still a distinct difference of fluctuation between the simulation and the crystal B-factors. In the simulation, higher fluctuations are observed at residues 111–118, where lower fluctuations according to the crystal B-factors are seen. The simulations from the other four systems also suggest that this region is flexible (Fig. 5). The crystallographic B-factors show in this region less flexibility and that may result from the crystal packing arrangement, which limits the flexibility of certain regions.

Figure 5 shows the RMSF profile of C_α atoms of the five simulations relative to their own average structures. The RMSFs of substrate-bound TyrRSs are compared to that of unliganded TyrRS respectively. There are three high flexibility regions where at least a peak value of RMSFs in one of the five simulations is larger than 1.8 Å, except for the residues from the two terminals. These three regions comprise residues 114–118, 128–134 and 225–238 respectively. We designate these three regions by HF1, HF2 and HF3.

Flexibility differences in the HF1 region (114–118)

The residues in the HF1 region are those loop residues connecting helix-5 and strand-4. The high flexibility in this region is not observed in the experimental B-factors. The corresponding residues of the unliganded TyrRS system display the highest fluctuations among the five systems. The binding of Tyr and tyrosyl adenylate does not alter the fluctuations very much; nevertheless, the binding of ATP and SB284484 increase the peak values of RMSFs by 1.0 and 0.7 Å respectively. The distances between the substrates and the residues in the middle of this loop are about

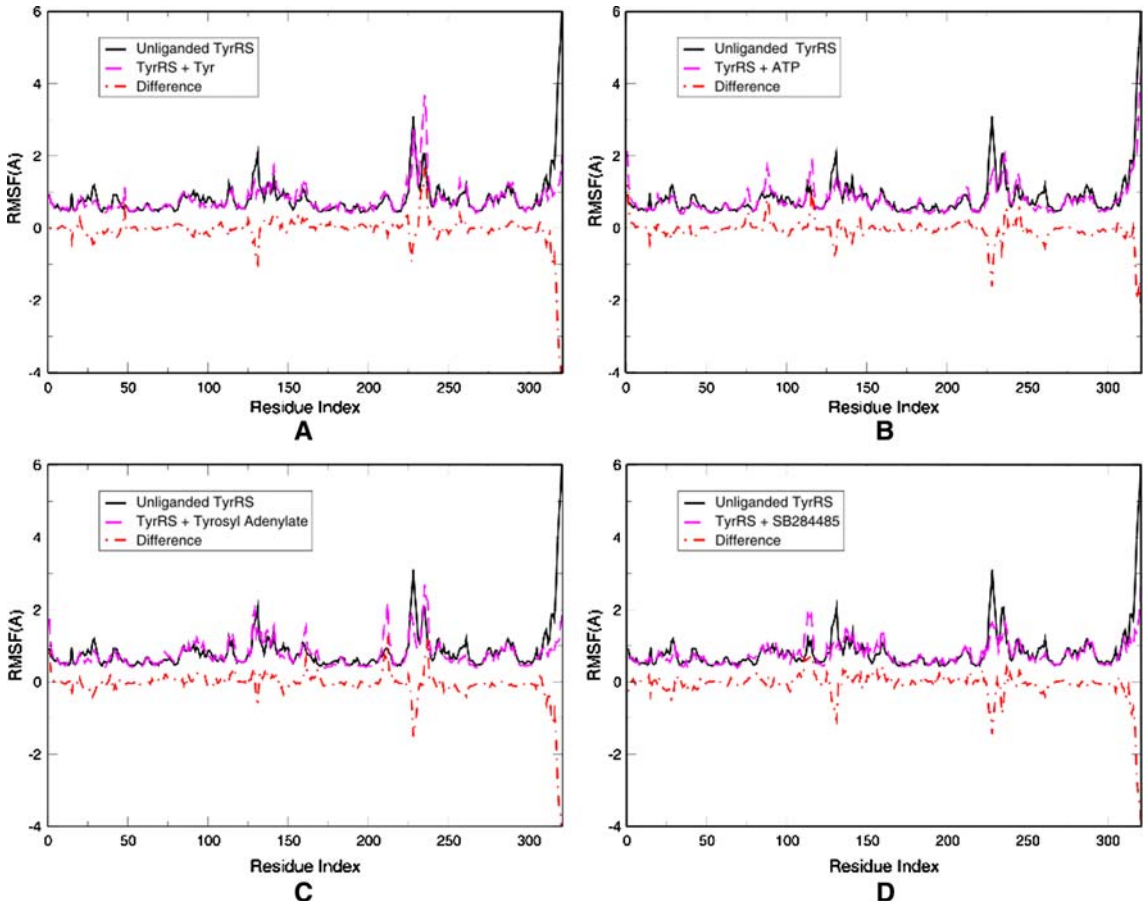

Fig. 5 Comparison of RMSFs of C_α atoms per residue between substrate-bound and unliganed TyrRS during the last 5 ns simulations. Differences of RMSFs are shown in *red dashed line*

22 Å. Obviously, the residues in this region do not belong to the binding site of these substrates. Therefore, the change of flexibility after the binding of different substrates must be communicated to the HF1 region through long-range interactions.

Flexibility differences in the HF2 region (128–133)

The HF2 region mainly includes a small loop (129–132) connecting helix-6 and helix-7. The residues in this region from the unliganded TyrRS system are characterized by the largest fluctuation value up to 2.0 Å at residue 132. The binding of tyrosyl adenylate shifts the peak value from residue 132 to 130 with the same magnitude. The peak values of fluctuations in the Tyr-bound, ATP-bound TyrRS and SB284485-bound systems go down to 1.27, 1.42 and 1.07 Å respectively.

Flexibility differences in the HF3 region (226–238)

The HF3 region includes most residues of the linker peptide and the KMSKS motif (residues 231–235) belongs also to this region. It is noteworthy that this region exhibits the highest difference in fluctuations compared to the HF1 and HF2 regions. The high flexibility is in agreement with the role played by the KMSKS loop in the catalysis of the tyrosine activation reaction: the KMSKS loop makes successive conformational changes between the open, closed and semi-open forms during Tyr-AMP formation (Kobayashi et al. 2005; Kuratani et al. 2006). The RMSF curve (Fig. 5) shows two peak values around residues Gly229 and Glu236 respectively. Thus, we divided this high mobile region into two flexible parts: part1 (residues 226–232) and part2 (233–238). The residues of part1 in the unliganded TyrRS and Tyr-bound systems exhibit relatively higher flexibility with a top peak value of 3.11 and 2.73 Å respectively. The binding of ATP, tyrosyl adenylate and SB284485 lead the peak values of fluctuations to be lower than 2 Å, which reveals that the formation of ATP, tyrosyl adenylate and SB284485 complex restrict the mobility of part1. For part2, the binding of Tyr and tyrosyl-adenylate increase the peak value up to nearly 4 and 3 Å respectively. The significant flexibility of the region encompassing the KMSKS motif was also observed in

MetRS based on MD simulation (Budiman et al. 2007), which is critical for the aaRSs catalytic activity.

Substrate binding modes and hydrogen bond analysis

To gain a further structural understanding of the interaction between the four substrates and TyrRS, the average structures of the last 5 ns simulations for each complex system are calculated and the binding modes are shown in Fig. 6. The hydrogen bonds that occupy more than 40% time in the 5 ns period are listed in Table 2 and also labeled with black dashed lines in the interaction figures (Fig. 6).

The residues of the tyrosine-binding pocket are well conserved in bacteria. Tyr36, Asp177, Gln174, Gln196, Tyr170, Asp80 of *S. aureus* TyrRS correspond to Tyr34, Asp176, Gln173, Gln195, Tyr169, Asp78 of *B. stearothermophilus* TyrRS; Tyr37, Asp182, Gln179, Gln201, Tyr175, Asp81 of *E. coli* TyrRS. The spatial arrangement and the roles in tyrosine binding of these residues are also well conserved between *B. stearothermophilus* and *E. coli* TyrRS structures (Kobayashi et al. 2005). Statistical data of the MD shows that the hydrogen bond network formed by tyrosine and *S. aureus* TyrRS is almost the same as those of *B. stearothermophilus* TyrRS and *E. coli* TyrRS: Tyr36 and Asp 177 form hydrogen bond with the phenolic hydroxyl group of tyrosine and Gln174 and Tyr 170 forms hydrogen bond with the nitrogen of tyrosine (NH2). In contrast, Asp80 does not form stable hydrogen bond with the nitrogen of tyrosine and there is a new hydrogen bond between Asp40 and the carboxyl oxygen, which is different in *B. stearothermophilus* TyrRS and *E. coli* TyrRS. The tyrosyl moiety of tyrosyl adenylate and SB284485 is accommodated in the same deep pocket of *S. aureus* TyrRS as where tyrosine accommodates. Tyr36 and Asp177 still form stable hydrogen bonds with the phenolic hydroxyl group of the tyrosyl moiety, which is also in agreement with the *B. stearothermophilus* TyrRS and *E. coli* TyrRS. However, the nitrogens (NH2 and N10) of the tyrosyl moiety of tyrosyl adenylate and SB284485 prefer to form only one hydrogen bond with Gln174 and Tyr170 respectively.

In the crystal structure of *S. aureus* TyrRS complexed with SB284485, the carboxylate oxygen atoms (O16 and O17) are hydrogen bonded to the main-chain nitrogen of Asp40, as well as the side chain of His47. The former hydrogen bond mimics a phosphate oxygen atom in tyrosyl adenylate. These two hydrogen bonds also appear during the simulation. At the same time, another possible hydrogen bond between the carboxylate oxygen atom and the side chain of His50 is found. Of the four phosphate oxygens in tyrosyl-adenylate, OP1 forms the closest interaction with residues of *B. stearothermophilus* TyrRS (Brick et al. 1989). This interaction is with the nitrogen of Asp38, and at 3.40 Å is relatively long to contribute significant hydrogen bonding energy (Brick et al. 1989). The average distance of this hydrogen bond is about 0.5 Å shorter in *S. aureus* TyrRS than *B. stearothermophilus* TyrRS. As we mentioned above, Asp40 also forms a hydrogen bond with

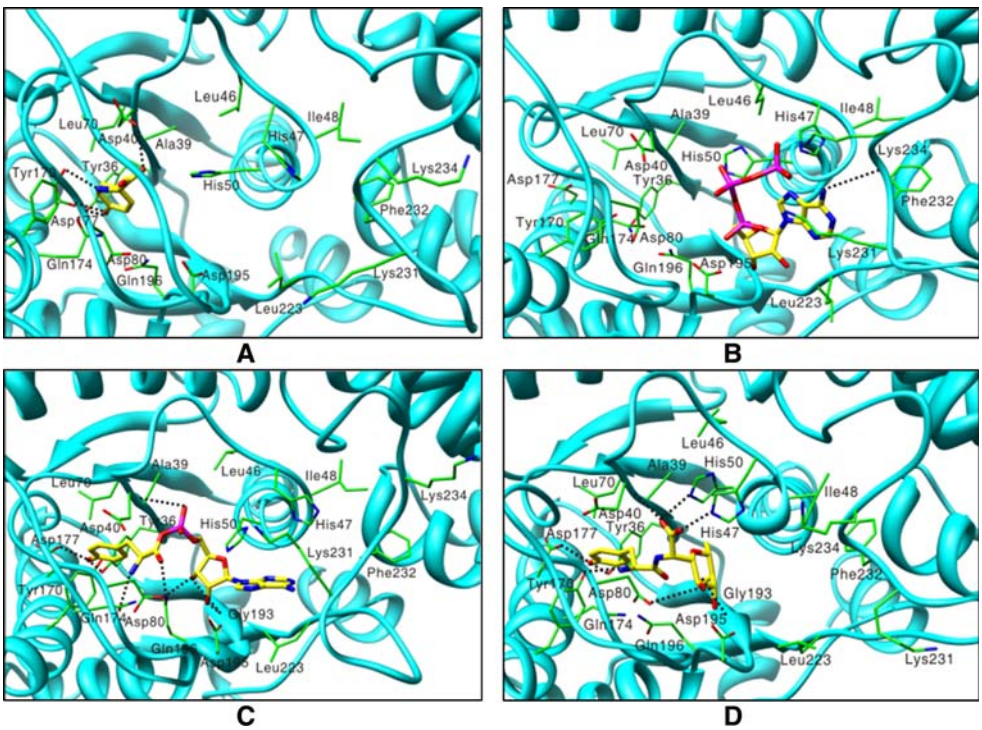

Fig. 6 Average structures and hydrogen bond network from the last 5 ns simulation of each substrate-bound TyrRS. The backbones of TyrRS are shown in *cyan ribbon* and side-chains of binding site residues are shown in *green stick*, respectively. Carbon atoms of the substrates are colored in *yellow*. Oxygen is in *red*, Nitrogen is in *blue* and Phosphorus is in *magenta*. Hydrogen bonds are displayed in *black dashed line*. **a** Tyr-bound TyrRS, **b** ATP-bound TyrRS, **c** Tyrosyl-adenylate-bound TyrRS, **d** SB284485-bound TyrRS

Table 2 Hydrogen bonds in substrates-bound TyrRS complex based on the last 5 ns simulations

(A) Hydrogen bond			Percentage occupied	Distance
TyrRS residues		Tyr		
Tyr36-OH	–	OH	95.48	3.039 (0.17)
Asp177-OD1	–	HO	86.20	2.767 (0.15)
Tyr170-HO	–	HNH2	63.61	3.125 (0.18)
Asp40-NH	–	OD1	55.48	3.043 (0.20)
(B) Hydrogen bond			Percentage occupied	Distance
TyrRS residues		ATP		
Phe232-O	–	H1N6	48.93	3.003 (0.17)
(C) Hydrogen bond			Percentage occupied	Distance
TyrRS residues		Tyrosyl adenylate		
Asp177-OD2	–	HO	99.81	2.696 (0.14)
Gly193-NH	–	O2′	96.00	2.979 (0.14)
Gln196-OE1H	–	O3′	94.33	2.921 (0.21)
Tyr36-OH	–	OH	83.57	3.052 (0.20)
Gly193-NH	–	O3′	68.82	3.238 (0.16)
Asp40-NH	–	OP1	57.06	3.208 (0.17)
Gln196-NE2H1	–	O	47.26	2.956 (0.16)
Gln174-OE1	–	HNH2	45.58	2.950 (0.17)
(D) Hydrogen bond			Percentage occupied	Distance
TyrRS residues		SB284485		
Asp177-OD2	–	HO	99.99	2.651 (0.11)
Asp40-NH	–	O16	89.61	2.912 (0.14)
Tyr36-OH	–	OH	75.77	2.995 (0.19)
Tyr170-HO	–	HN10	75.37	3.062 (0.16)
Gly193-NH	–	O26	72.78	3.012 (0.16)
Asp80-OD2	–	HO24	49.64	2.669 (0.12)
His50-NE2HE2	–	O16	44.60	3.037 (0.17)
His47-NE2HE2	–	O17	40.95	2.968 (0.19)

(A) Tyr-bound TyrRS, (B) ATP-bound TyrRS, (C) Tyrosyl-adenylate-bound TyrRS, (D) SB284485-bound TyrRS

the carboxyl oxygen of tyrosine. Thus, Asp40 seems to play a more important role in *S. aureus* TyrRS.

It has been reported that there are hydrogen bonds between 2′-OH of the ribosyl moiety of tyrosyl adenylate and the main-chain nitrogen of Gly192 and the carboxylate of Asp194 of *B. stearothermophilus* TyrRS (Brick et al. 1989). Moreover, 2′-OH of the ribosyl moiety of Tyr-AMS hydrogens bond with the corresponding main-chain NH group of Gly198 and with the side-chain of Asp 200 of *E. coli* TyrRS (Kobayashi et al. 2005). According to our MD analysis, the main-chain nitrogen of Gly193 of *S. aureus* TyrRS also forms the same hydrogen bond with the 2′-OH of the ribosyl moiety of tyrosyl adenylate, however, the corresponding Asp195 does not form the same hydrogen bond. The 3′-OH of the ribosyl moiety of tyrosyl adenylate from *B. stearothermophilus* TyrRS interacts with a water molecule by hydrogen bond, which is not found in *S. aureus* TyrRS based on our simulations. Instead, Gln196 replaced the water molecule to form the hydrogen bond with 3′-OH of the ribosyl moiety. One hydroxyl group of SB284485 imitate the 2′-OH of the ribosyl moiety of tyrosyl adenylate to form stable hydrogen bonds with Gly193, while another forms a hydrogen bond with the carboxylate oxygen of Gln174. The hydroxyl group of the ribose moiety of ATP reveals no hydrogen bond with the residues of *S. aureus* TyrRS.

The difference in the adenine moiety recognition is large between *E. coli* TyrRS and *B. stearothermophilus* TyrRS, while the tyrosyl moiety is recognized similarly (Kobayashi et al. 2005). The adenine ring is recognized by the hydrogen bonds in the *E. coli* TyrRS. The adenine moiety of tyrosyl adenylate makes no significant hydrogen bond interaction in *S. aureus* TyrRS according to the simulation, which has the same characteristics as that in *B. stearothermophilus* TyrRS (Brick et al. 1989). The adenine moiety of ATP rotates almost 90° in the clockwise direction around the bond connecting the ribose moiety compared to the situation in tyrosyl adenylate, which is possibly due to the presense of the hydrogen bond between N6 and the main-chain oxygen of Phe232.

The dynamics of the KMSKS loop

Structural studies of the bacterial TyrRSs from *B. stearothermophilus*, *E. coli*, *T. thermophilus* revealed that the KMSKS loops adopt different conformations (Brick and Blow 1987; Brick et al. 1989; Kobayashi et al. 2005; Yaremchuk et al. 2002). The induced-fit conformational rearrangement of the flexible KMSKS loop occurs during the catalysis of Tyr-AMP formation. The KMSKS loop makes successive conformational changes between open, closed, and semi-open forms during Tyr-AMP formation. Moreover, the open conformation occurs when tyrosine binds to TyrRS. After ATP binding, KMSKS loop moves toward the active site to fix ATP in a closed conformation. Following Tyr-AMP formation, the KMSKS loop shifts away from the active site, in a semi-open conformation which allows tRNA CCA end to easily access the aminoacyl transfer center (Kuratani et al. 2006). It has been designated that the KMSKS loop adopts open, semi-open and open forms in the *E. coli* TyrRS·tyrosine, *E. coli* TyrRS·Tyr-AMS and *T. thermophilus* TyrRS·ATP·tyrosinol·$tRNA^{Tyr}$ respectively (Kobayashi et al. 2005). Figure 7a shows the conformational changes of the KMSKS loop after superposing the three experimental complexes. The semi-open

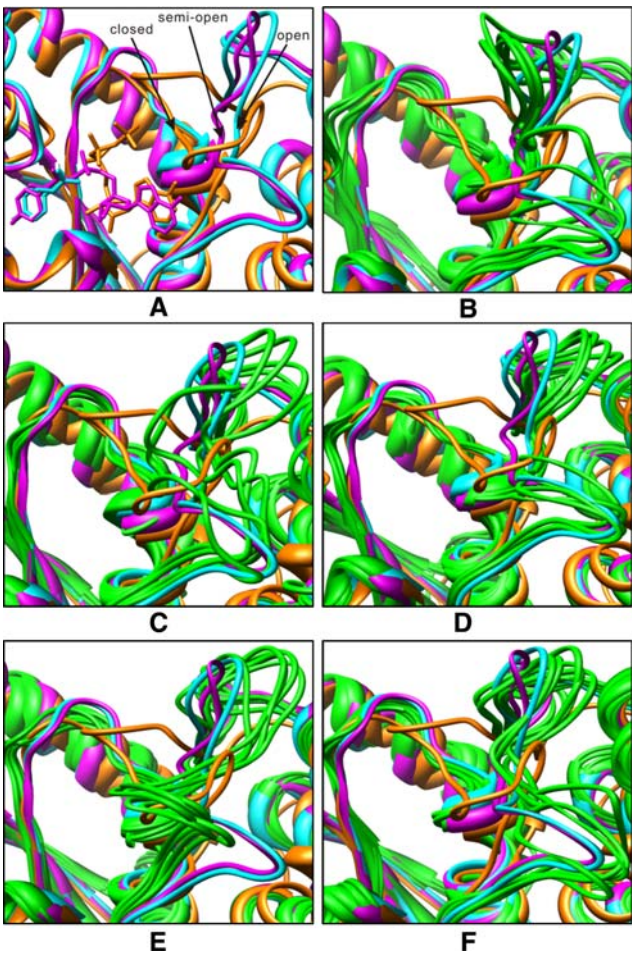

Fig. 7 Conformational changes of the KMSKS loop. **a** open, semi-open and closed conformations of the KMSKS loop in the *E. coli* TyrRS·tyrosine (*cyan*), *E. coli* TyrRS·Tyr-AMS (*magenta*) and *T. thermophilus* TyrRS·ATP·tyrosinol·tRNA^{Tyr} (*orange*) respectively. **b–f** Superposition of each five snapshots (*green*) from the last 5 ns simulation with a 1 ns interval of the five simulated TyrRS systems on the *E. coli* TyrRS·tyrosine, *E. coli* TyrRS·Tyr-AMS and *T. thermophilus* TyrRS·ATP·tyrosinol·tRNA^{Tyr}. Snapshots are from **b** unliganded TyrRS **c** Tyr-bound TyrRS **d** ATP-bound TyrRS **e** Tyrosyl-adenylate-bound TyrRS **f** SB284485-bound TyrRS

conformation of KMSKS loop locates between the open and closed conformations and looks a little more like the open conformation.

Most of the dynamical information of the KMSKS loop comes from the comparison of crystal structures among the same or different species and seldom from the comparison of dynamical structures in the same species. Although it is impossible to uncover the secret of the KMSKS loop moving of *S. aureus* TyrRS completely due to the limitation of simulation time, the MD analysis still can give some useful information about the mobility of KMSKS loop. The KMSKS loops of substrate-free *S. aureus* TyrRS (Fig. 7b) and ATP-bound *S. aureus* TyrRS (Fig. 7d) actually adopts the open conformation. According to the dynamics data, ATP binding did not transiently induce closed forms, although it induces the closed forms of KMSKS loop of *T. thermophilus* TyrRS (Yaremchuk et al. 2002). We should note that the closed form appears after the binding of both tyrosinol and ATP in *T. thermophilus* TyrRS. It seems that the closed conformation may only appear when Tyr and ATP bind to *S. aureus* TyrRS simultaneously because the combination binding of Trp and ATP is also necessary for efficient induced-fit of TrpRS (Kapustina and Carter 2006). The open conformation induced only by ATP enlarges the entrance to the tyrosine binding pocket, which may facilitate the binding of tyrosine. The KMSKS loop of Tyr-bound TyrRS (Fig. 7c) shifts in a large magnitude between semi-open and open conformations. The KMSKS loop in *B. stearothermophilus* and *E. coli* TyrRS display open conformations with the binding of tyrosine in the crystal structures (Brick et al. 1989; Kobayashi et al. 2005). Our simulations suggest the binding of Tyr may also induce the KMSKS loop to adopt a semi-open conformation in *S. aureus* TyrRS. Furthermore, it can also be observed that the binding of tyrosyl adenylate induces the first two KF residues of the KMSKS loop to twist in an anticlockwise direction and in a conformation similar to the closed conformation, while those of the last three GKS residues in a conformation near to a semi-open and open conformation (Fig. 7e). As after the Tyr-AMP formation, the KMSKS loop of *E. coli* TyrRS shifts away from the active site and turns to semi-open form which may be related to the binding and guiding of the CCA end of tRNA^{Tyr} for the aminoacyl transfer reaction (Kobayashi et al. 2005), the semi-open and open conformation of latter three GKS residues of KMSKS loop in *S. aureus* TyrRS may be probably involved in the initial tRNA binding. In the end, upon the inhibitor SB284485 binding, the KMSKS loop of *S. aureus* TyrRS exhibits a semi-open conformation (Fig. 7f).

Conclusion

In this study, we have analyzed the dynamic behavior of *S. aureus* TyrRS with and without substrates in detail, in an effort to understand the conformational changes involved in the catalytic mechanism of the activation of tyrosine by TyrRS. One 14 ns and four 12 ns MD simulations of TyrRS in its free form and complexed with Tyr, ATP, tyrosyl adenylate and an inhibitor (SB284485) respectively have been carried out. According to the statistical analysis of RMSD data, the last 5 ns simulations of each system which are more stable were selected to do further analysis.

The results of RMSDs of the C_α atoms and radius of gyration show that substrate-free TyrRS samples more relaxed conformational space than substrate-bound TyrRS. We found three regions (HF1, HF2, HF3) with high

flexibility which encompasses residues 114–118, 128–133, and 226–238 respectively. The HF3 region which includes the KMSKS motif shows the highest difference in fluctuations among the five trajectories compared to HF1 and HF2 regions. The significant flexibility of the HF3 region is critical for TyrRS catalytic activity.

The average structures and occupied time of hydrogen bonds for the last 5 ns simulations were calculated. Our MD simulations show that the hydrogen bond network formed by tyrosine and *S. aureus* TyrRS is similar as those of *B. stearothermophilus* TyrRS and *E. coli* TyrRS. The tyrosyl moiety of tyrosyl adenylate and SB284485 is accommodated in the same deep pocket of *S. aureus* TyrRS as where tyrosine accommodates. Tyr36 and Asp177 still form stable hydrogen bond with the phenolic hydroxyl group of tyrosyl moiety. However, the nitrogens of tyrosyl moiety of tyrosyl adenylate and SB284485 prefer to form only one hydrogen bond with Gln174 and Tyr170 respectively. Moreover, one hydroxyl group of SB284485 imitate the 2′-OH of the ribosyl moiety of tyrosyl adenylate to form stable hydrogen bonds with Gly193, while another forms a hydrogen bond with the carboxylate oxygen of Gln174. The hydroxyl group of ribose moiety of ATP and the adenine moiety of tyrosyl adenylate reveals no hydrogen bond with the residues of *S. aureus* TyrRS.

Analysis of the dynamics reveals that different substrates induce the rearrangement of the KMSKS loop. The KMSKS loop of substrate-free *S. aureus* TyrRS adopts an open conformation. The tyrosine binds to the pocket with the KMSKS loop shifting between semi-open and open forms. The ATP binding still induces the KMSKS loop into the open form. After the Tyr-AMP is formed, the former two KF residues of KMSKS loop twist in an anticlockwise direction and in a conformation similar to a closed conformation, while the latter three GKS residues adopt semi-open and open conformation which may probably be involved in the initial tRNA binding.

References

Berman HM, Westbrook J, Feng Z, Gilliland G, Bhat TN, Weissig H et al (2000) The protein data bank. Nucleic Acids Res 28:235–242. doi:10.1093/nar/28.1.235

Bhat TN, Blow DM, Brick P, Nyborg J (1982) Tyrosyl-tRNA synthetase forms a mononucleotide-binding fold. J Mol Biol 158:699–709. doi:10.1016/0022-2836(82)90255-8

Bonnefond L, Giege R, Rudinger J (2005) Evolution of the $tRNA^{tyr}$/TyrRS aminoacylation systems. Biochimie 87:873–883. doi:10.1016/j.biochi.2005.03.008

Brick P, Blow DM (1987) Crystal structure of a deletion mutant of a tyrosyl-tRNA synthetase complexed with tyrosine. J Mol Biol 194:287–294. doi:10.1016/0022-2836(87)90376-7

Brick P, Bhat TN, Blow DM (1989) Structure of tyrosyl-tRNA synthetase refined at 23 Å resolution. Interaction of the enzyme with the tyrosyl-adeylate intermediate. J Mol Biol 208:83–98. doi:10.1016/0022-2836(89)90090-9

Budiman ME, Knaggs MH, Fetrow JS, Alexander RW (2007) Using molecular dynamics to map interaction networks in an aminoacyl-tRNA synthetase. Proteins 68:670–689. doi:10.1002/prot.21426

Carter P, Bedouelle H, Winter G (1986) Construction of heterodimer tyrosyl-tRNA synthetase shows $tRNA^{Tyr}$ interacts with both subunits. Proc Natl Acad Sci USA 83:1189–1192. doi:10.1073/pnas.83.5.1189

Case DA, Darden TA, Cheatham TEIII, Simmerling CL, Wang J, Duke RE et al (2006) AMBER 9. University of California, San Francisco

Dadarlat VM, Post CB (2001) Insights into protein compressibility from molecular dynamics simulations. J Phys Chem B 105:715–724. doi:10.1021/jp0024118

Darden T, York D, Pedersen L (1993) Particle mesh Ewald: an NLog(N) method for Ewald sums in large systems. J Chem Phys 98:10089–10092. doi:10.1063/1.464397

Duan Y, Wu C, Chowdhury S, Lee MC, Xiong G, Zhang W et al (2003) A point-charge force field for molecular mechanics simulations of proteins based on condensed-phase quantum mechanical calculations. J Comput Chem 24:1999–2012. doi:10.1002/jcc.10349

Eriani G, Delarue M, Poch O, Gangloff J, Moras D (1990) Partition of tRNA synthetases into two classes based on mutually exclusive sets of sequence motifs. Nature 347:203–206. doi:10.1038/347203a0

Fersht AR, Knill-Jones JW, Bedouelle H, Winter G (1988) Reconstruction by site-directed mutagenesis of the transition state for the activation of tyrosine by the tyrosyl-tRNA synthetase: a mobile loop envelopes the transition state in an induced-fit mechanism. Biochemistry 27:1581–1587. doi:10.1021/bi00405a028

Gohlke H, Kuhn LA, Case DA (2004) Change in protein flexibility upon complex formation: analysis of Ras–Raf using molecular dynamics and a molecular framework approach. Proteins 56:322–337. doi:10.1002/prot.20116

Hountondji C, Dessen P, Blanquet S (1986) Sequence similarities among the family of aminoacyl-tRNA synthetases. Biochimie 68:1071–1078. doi:10.1016/S0300-9084(86)80181-X

Hughes SJ, Tanner JA, Miller AD, Gould IR (2006) Molecular dynamics simulations of LysRS: a asymmetric state. Proteins 62:649–662. doi:10.1002/prot.20609

Ibba M, Soll D (2000) Aminoacyl-tRNA synthesis. Annu Rev Biochem 69:617–650. doi:10.1146/annurev.biochem.69.1.617

Jakalian A, Bush BL, Jack DB, Bayly CI (2000) Fast, efficient generation of high-quality atomic charges AM1-BCC model: I Method. J Comput Chem 21:132–146. doi:10.1002/(SICI)1096-987X(20000130)21:2<132::AID-JCC5>3.0.CO;2-P

Jorgensen WL (1982) Revised TIPS for simulations of liquid water and aqueous solutions. J Chem Phys 77:4156–4163. doi:10.1063/1.444325

Jorgensen WL, Chandrasekhar J, Madura JD, Impey RW, Klein ML (1983) Comparison of simple potential functions for simulating liquid water. J Chem Phys 79:926–935. doi:10.1063/1.445869

Kapustina M, Carter CW (2006) Computational studies of Tryptophanyl-tRNA synthetase: activation of ATP by induced-fit. J Mol Biol 362:1159–1180. doi:10.1016/j.jmb.2006.06.078

Kobayashi T, Nureki O, Ishitani R, Yaremchuk A, Tukalo M, Cusack S et al (2003) Structural basis for orthogonal tRNA specificities of tyrosyl-tRNA synthetases for genetic code expansion. Nat Struct Biol 10:425–429. doi:10.1038/nsb934

Kobayashi T, Takimura T, Sekine R, Vincent K, Kamata K, Sakamoto K et al (2005) Structural snapshots of the KMSKS loop rearrangement for amino acid activation by bacterial

tyrosyl-tRNA synthetase. J Mol Biol 346:105–117. doi:10.1016/j.jmb.2004.11.034

Kuratani M, Sakai H, Takahashi M, Yanagisawa T, Kobayashi T, Murayama K et al (2006) Crystal structures of tyrosyl-tRNA synthetases from Archaea. J Mol Biol 355:395–408. doi:10.1016/j.jmb.2005.10.073

McCammon JA, Harvey SC (1987) Dynamics of proteins and nucleic acids. Cambridge University Press, Cambridge

Ochsner UA, Sun X, Jarvis T, Critchley I, Janjic N (2007) Aminoacyl-trna synthetases: essential and still promising targets for new anti-infective agents. Expert Opin Investig Drugs 16:573–593. doi:10.1517/13543784.16.5.573

Pearlman DA, Case DA, Caldwell JW, Ross W, Cheatham TEIII, DeBolt S et al (1995) AMBER, a package of computer programs for applying molecular mechanics, normal mode analysis, molecular dynamics and free energy calculations to simulate the structural and energetic properties of molecules. Comput Phys Commun 91:1–41. doi:10.1016/0010-4655(95)00041-D

Pettersen EF, Goddard TD, Huang CC, Couch GS, Greenblatt DM, Meng EC et al (2004) UCSF chimera—a visualization system for exploratory research and analysis. J Comput Chem 25:1605–1612. doi:10.1002/jcc.20084

Qiu X, Janson CA, Smith WW, Green SM, McDevitt P, Johanson K et al (2001) Crystal structure of *Staphylococcus aureus* tyrosyl-tRNA synthetase in complex with a class of potent and specific inhibitors. Protein Sci 10:2008–2016. doi:10.1110/ps.18001

Retailleau P, Yin Y, Hu M, Roach J, Bricogne G, Vonrhein C et al (2001) High-resolution experimental phases for tryptophanyl-tRNA synthetase (TrpRS) complexed with tryptophanyl-5′AMP. Acta Crystallogr D Biol Crystallogr 57:1595–1608. doi:10.1107/S090744490101215X

Ryckaert JP, Ciccotti G, Berendsen HJC (1977) Numerical integration of the cartesian equations of motion of a system with constraints: molecular dynamics of *n*-alkanes. J Comput Phys 23:327–341. doi:10.1016/0021-9991(77)90098-5

Thompson D, Simonson T (2006) Molecular dynamics simulations show that bound Mg^{2+} contributes to amino acid and aminoacyl adenylate binding specificity in aspartyl-tRNA synthetase through long range electrostatic interactions. J Biol Chem 281:23792–23803. doi:10.1074/jbc.M602870200

Thompson D, Plateau P, Simonson T (2006) Free-energy simulations and experiments reveal long-range electrostatic interactions and substrate-assisted specificity in an aminoacyl-tRNA synthetase. Chembiochem 7:337–344. doi:10.1002/cbic.200500364

Wang J, Wolf RM, Caldwell JW, Kollman PA, Case DA (2004) Development and testing of a general amber force field. J Comput Chem 25:1157–1174. doi:10.1002/jcc.20035

Winter G, Koch GL, Hartley BS, Barker DG (1983) The amino acid sequence of the tyrosyl-tRNA synthetase from *Bacillus stearothermophilus*. Eur J Biochem 132:383–387. doi:10.1111/j.1432-1033.1983.tb07374.x

Xin Y, Li WD, First EA (2000) Stabilization of the transition state for the transfer of tyrosine to $tRNA^{Tyr}$ by tyrosyl-tRNA synthetase. J Mol Biol 303:299–310. doi:10.1006/jmbi.2000.4126

Yaremchuk A, Kriklivyi I, Tukalo M, Cusack S (2002) Class I tyrosyl-tRNA synthetase has a class II mode of cognate tRNA recognition. EMBO J 21:3829–3840. doi:10.1093/emboj/cdf373